Available online at www.sciencedirect.com

ScienceDirect

Procedia Computer Science 158 (2019) 177–197

Procedia Computer Science

www.elsevier.com/locate/procedia

3rd World Conference on Technology, Innovation and Entrepreneurship (WOCTINE)

Simulation-Based Parametric Study for the Hybrid Superplastic Forming of AZ31

Fatima Ghassan Al-Abtah[a,*], Naser Al-Huniti[b], Elsadig Mahdi[a]

[a] Qatar University, Doha 2713, Qatar

[b] University of Jordan, Amman, Jordan

Abstract

As the lightest constructional metal on earth, magnesium alloys offer excellent potential for weight reduction in the transportation industry and it was observed that some magnesium alloys exhibit superior ductility and superplastic behaviour at high temperatures. The main limitation of the Superplastic forming (SPF) includes the low production rate since it needs a long forming time for each part. Through this study, an SPF process that starts with a mechanical pre-forming stage is developed to promote formability and reduce forming time. A two-dimensional finite element model is used to simulate the process. The forming process consists of two steps. At the pre-forming step (deep drawing), the sheet is drawn into the die to a preselected level, using a mechanical punch, and at the second step (SPF) a pressurized gas is applied at a controlled rate. It is shown that a significant reduction in forming time and improved final thickness uniformity can be achieved when the hybrid forming technique is used, where the process achieved a fully formed part at 400°C. Investigation for the impact of different forming process parameters achieved by comparing forming time and the distribution of final thickness that were obtained from the simulation analysis. Maximum thinning decreased from over 67% to less than 55% and forming time significantly decreased by more than 6 minutes, and the required gas pressure profile was predicted for optimum forming process parameters based on the 0.001/sec target constant strain rate within the sheet.

Peer-review under responsibility of the scientific committee of the 3rd World Conference on Technology, Innovation and Entrepreneurship

Keywords: Finite element analysis; Magnesium; Plasticity; Superplastic forming

1877-0509
Peer-review under responsibility of the scientific committee of the 3rd World Conference on Technology, Innovation and Entrepreneurship
10.1016/j.procs.2019.09.041

1. Introduction

Superplastic forming (SPF) is a metalworking process where material can elongate beyond 200% of the original size [2]. The primary requirement for attaining superplasticity is avoiding processes that limit elongation in tensile deformation or biaxial stretch forming: plastic instability (necking) and fracture [29]. Three main requirements generally needed to achieve superplastic behavior in the material. These are fine and stable grain sizes in the submicron range, where superplasticity is known as strong grain size dependent phenomenon. The grain sizes for superplastic metals are required to be less than 10 micrometers using a high, homologous temperature and deformation under stress with a small mean normal component [5]. By combining the effects of both the grain size and temperature, it is generally believed that the smaller the grain size, the lower the temperature that can be used to achieve superplasticity, and vice versa [1]. Those materials that meet these parameters must still have a strain rate sensitivity which is a measurement of the way the stress on a material reacts to changes in strain rate of >0.3 to be considered superplastic.

Hybrid superplastic forming method (HSPF) is a combination of mechanical performing with superplastic forming. This method has taken advantage of both the benefits of deep drawing and superplastic forming. It is through this method that the low forming rates of conventional superplastic forming can be overcome and the forming temperature can be lowered. Main practice for both SPF and HSPF is based on trial and error, so through this paper, a predictive tool will be presented to avoid the usage of the trial and error methods, recent advancements in finite element tools have helped in the analysis of complex SPF operations. These tools can be utilized successfully to develop optimized SPF techniques. Superplastic forming is utilized to form superplastic materials into parts with intricate geometries in a single manufacturing step. The finished product has excellent precision and a fine surface finish. It also does not suffer from spring back or residual stresses. Magnesium alloys are applicable in many applications where weight savings are essential since they have high strength and low density. Since early 1980, several commercially available alloys have been developed for use in aerospace structures including helicopter transmission units [23] [6]. The superplastic forming mechanism is currently utilized to form lightweight combined components without the need for fasteners or joining operations. Those are essential characteristics especially in the automotive industry; where there is a high demand to produce lighter weight cars due to the high gas prices and the greenhouse effect. The hybrid SPF can be commercially applicable to stratify on the high production rates, particularly for the technology that is meant to save energy. The reduced forming temperature will give a lower carbon footprint by the incorporation of a technology that saves energy.

Analytical analysis of the superplastic forming was first started for a thin circular diaphragm [11]. On the other hand, the superplastic forming of a long rectangular box section of Ti-6Al-4V was simulated by developing a numerical analysis, where the necessary pressure to preserve a constant strain rate was predicted [8]. In a more recent study, and utilizing the advancements in the finite element method, the impact was compared by utilizing several element types on the simulation of the superplastic forming of SPF grade of AA5083 into a long rectangular box [18]. Furthermore, research was established to study the effect of die geometry and friction on the results of simulation [9]. A bulge forming of AA5083 was simulated under high-temperature quick-plastic forming (QPF) conditions with constant pressure profiles from experiments, where the importance of including material hardening/softening in the material model that was demonstrated [10]. Further studies based on the material model developed by [10], investigated the effects of interfacial friction between the die and the sheet on the integrity of superplastically formed parts. A dimensionless analysis of superplastic bulge forming was applied to reduce the number of variables involved in the SPF process to facilitate its characterization where a constant pressure has been assumed, and it was shown that dimensional analysis could be a useful tool for describing SPF processes [12]. The particle swarm-optimization-method was used for the constitutive modeling of AZ31B, and High-temperature bulge experiments were used to validate the model. Results indicated that the suggested power law model grants high predictions accuracy for the lower strain rates [30].A process that incorporates hot draw mechanical pre-forming (HDMP) with superplastic forming was developed by [17]. Both strain and strain rate has been used in the power law equation to model the material for the HDMP of an SPF5083 alloy. Three-dimensional explicit finite element code LS-DYNA was employed to incorporate the operation, where a simple square die was utilized for the preliminary study. The effect of several forming process parameters was examined by comparing the distribution of the final thickness from the simulation study of the SPF5083 alloy, where they found that higher depth of draw or increased punch sizes give a refinement in

the final thickness profile. They delivered an excellent thickness profile where maximum thinning and forming time was decreased.

The FEM was used to simulate a process that combines mechanical pre-forming with SPF by utilizing the non-superplastic material AA5083-O, where a general creep equation based on tensile test data was adopted as a material model for the simulation [15]. The influence of different process parameters was inspected by comparing the final sheet thickness and level of material draw-in. It was proved that a uniform formed part could be obtained by using the punch with higher depth during the mechanical pre-forming phase. Since it is critical to determine the material parameters during superplastic forming of AA 5086 Alloy, a steady state equation was derived to determine the approximate time for the sheet metal to attain the set temperature and also determined the most favorable temperature and pressure necessary for achieving the deformation of the workpiece based on equal thickness distribution [27]. A 2-dimensional finite element model was used to simulate a hybrid forming process that consists of two steps using a simple material model. In the first step, the Mg AZ31 sheet was drawn into the die isothermally using a mechanical punch, and then a pressurized gas was applied to force the sheet to acquire the die details. They used the reverse free bulging step to tackle the specific issue of severe thinning and to reduce the forming time of Mg AZ31 alloy. Finally, it was shown that a significant reduction in forming time and improved final thickness uniformity could be achieved when the hybrid forming technique is used. However, the investigation did not include a parametric study or optimization of the process [20].

A greener manufacturing technique that combines drawing (mechanical pre-forming) with SPF was studied, where it fulfills the forming at a quicker rate and minimized temperature in one metis process. The forming time of the process was shortened from 30 to 8 minutes, and lowered the forming temperature from 773 to 673 K [13]. It was found that it is credible to utilize the HSPF process to form into three stepped die cavity at 673 K because of the little variance between 673 and 773 K when comparing the bulge heights. Forging was added to the superplastic forming to boost the forge ability of semi-continuously cast AZ70 magnesium alloy and recognize the application of the as-cast magnesium alloy in major deformation bullet shell. The products showed the high-quality surface, it exhibited a contented microstructure and excellent mechanical properties plus a 30% weight saving [21].

A review was presented on the improvements concerning the superplastic forming that been more utilized in the last decades. There was a summarized discussion about the QPF, which is a successful metal forming mechanism since it has faster forming times as compared to the previous forming techniques [25]. Nowadays, the interest in this phenomenon and its forming technique is growing up, and a large amount of literature and researches are available, expanding more to cover the various aspects of superplasticity; also, more significant numbers of different parts are being produced by the superplastic forming technique [1].

Nomenclature

σ	true stress (MPa)
K	material constant
$\dot{\varepsilon}$	strain rate
ε	true strain
m	strain rate sensitivity exponent
a	radius of the die
S	thickness after time *t*
S_0	original thickness
ρ	radius of curvature
P	applied pressure.
n	strain hardening exponent

* Corresponding author. Tel.: +974-55-620-623.
E-mail address: fa1310021@qu.edu.qa

2. Material Model Development and Verification

2.1 Material Model Development

In superplastic forming process, the materials undergo a viscoplastic deformation, where constitutive modelling of superplastic deformation depends on significant viscoplastic deformation, where the elastic strain is neglected since it is minimal compared to the plastic one. The flow stress relates to strain rate and strain. The stress/strain and strain rate relationship can be characterized using the power law equation.

$$\sigma = K\dot{\varepsilon}^m\varepsilon^n \tag{1}$$

The material alloy selected for the study was AZ31 magnesium alloy. The equation of both strain rate and the strain was found by the power curve fitting of a tensile data for an AZ31 alloy for different target strain rate and different strain rate sensitivity exponent each time, to finally compare between them and choose the most appropriate one with fewer errors between simulation and analytical results. The first material model that was used is without strain hardening. The material model was extracted from the experimental data of [1]. Table 1 gives an in-depth look at the connection that relates true stress to strain rate and the effect of increasing strain rates on the percent of elongation at fracture and on the strain rate sensitivity exponent, where it is shown that the percent of elongation at fracture decreases when strain rate increases.

Table1. Based on Experimental data of an AZ31 alloy without strain hardening [1]

Strain Rate	Flow Stress	m-value	Fracture True Strain	Percent Elongation
0.00005	2.0000	0.3140	1.7458	473.05
0.00010	3.0000	0.5850	1.6963	445.37
0.00020	5.0000	0.7370	1.6046	397.59
0.00050	10.5000	0.8097	1.4553	328.58
0.00100	16.5000	0.6521	1.3052	268.84
0.00250	24.5000	0.4314	1.1466	214.76
0.00500	29.0000	0.2433	1.1359	211.40
0.01000	33.0000	0.1864	0.9615	161.56

The power curve fitting was applied to the stress/strain rate curve to get the following material model without strain hardening ($\sigma = K\dot{\varepsilon}^m$), where:

- K= 1537
- m=0.6705

It was found that the relation between true stress and strain rate is linear in the case of the material model without strain hardening, which is not real. Therefore, it was more accurate to use a material model that includes the strain hardening effect. The form of the creep equation should be changed to the following form [4]:

$$\frac{d\varepsilon}{dt} = (\mathrm{A}\sigma^n[(m+1)\varepsilon]^m)^{\frac{1}{m+1}} \tag{2}$$

Where A, m and n are the input parameters into the ABAQUS, they were found by finding the relation between them and K, m and n as follows, but to make it less confusing, K, m and n will be changed to B, X, and Y respectively.

- $n = \frac{1}{X+Y} = 1.4914,$ (3)
- $m = \frac{-Y}{X+Y} = 0,$ (4)
- $A = \frac{1}{B^n(m+1)^m} = 1.7676\times10^{-5}$, (5)

2.2 Material Model Verification

The capabilities of the model will be tested in bulge forming operations being the most common of all using pressurized gas where the selection of the forming pressure-time profile is very critical to achieve the maximum deformation without failure. Finite element simulation of the process has been performed using the commercial finite element solver ABAQUS. User-defined subroutines were compiled to implement the constitutive model into the FE code. A built-in pressure control algorithm was used in the analysis to generate the forming pressure profiles. A schematic of the free bulge forming process is shown in figure1 [1], where pressure P was applied at one side of the circular sheet, allowing the formation of a complete hemisphere of radius r_0 on the other side.

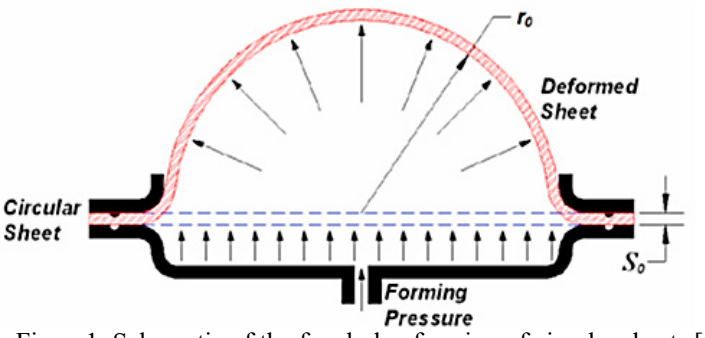

Figure1: Schematic of the free bulge forming of circular sheets [1]

2.3 Simulation Results

Circular sheet with a thickness of 1.04 mm was bulged to form a full hemisphere of 31.75 mm in height for a strain rate of 1×10^{-3} 1/s. The sheet was divided into four layers with 300 elements per layer; the element type was chosen to be CAX4I which is a 4-node bilinear incompatible modes element. One-half of the die is applied in section view since symmetry was used in the simulation. The initial pressure was chosen to be 0.0005 MPa, 0.000001 MPa minimum pressures, and 900 MPa maximum pressures. The Modulus of elasticity of magnesium is 45000 MPa and Poisson's ratio is 0.35. The analysis stopped when the spatial displacement at pole node in the y-direction reached 31.75 mm, where the forming time at that point was found to be 14.75 min while in experimental bulge forming for the same alloy and same strain rate the forming time was 14.68 min [1]. The thickness distribution was found by taking the coordinate data for the elements of both the top and bottom of the sheet and then finding the distance in each element. Figure2 shows thickness distributions concerning the position along the die surface.

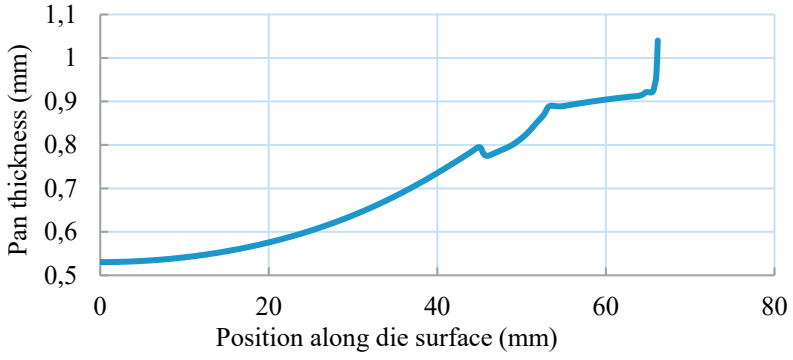

Figure2: thickness distribution with respect to the position along die surface

Finally, it was found that the model has an average thickness of 0.7048 mm, a minimum thickness of 0.5303 and a thinning factor of 0.7525. To know whether those results are acceptable or not, it is a must to compare those simulation-based results with analytical results. Due to the geometrical simplicity of the bulge, it is possible to derive an analytical expression for thickness and pressure-time forming profile.

2.4 Analytical Results

According to [7] the following analytical expressions for the radius of curvature, the ratio of thickness to the radius of curvature and pressure respectively were introduced.

$$\rho = \frac{a}{2[\exp(-\dot{\varepsilon}t)(1-\exp(-\dot{\varepsilon}t))]^{1/2}}, \quad (6)$$

$$\frac{S}{\rho} = \frac{2S_0\exp(-\dot{\varepsilon}t)[\exp(-\dot{\varepsilon}t)(1-\exp(-\dot{\varepsilon}t))]^{1/2}}{a}, \quad (7)$$

$$P = 4\frac{S_0}{a}\bar{\sigma}\exp(-\dot{\varepsilon}t)\left[\exp(-\dot{\varepsilon}t)(1-\exp(-\dot{\varepsilon}t))\right]^{\frac{1}{2}}, \quad (8)$$

Where:

- a = 31.75mm.
- S_0 = 1.04 mm.

Figure3 shows the relation between the radius of curvature, the ratio of thickness to the radius of curvature and pressure with increasing of time respectively.

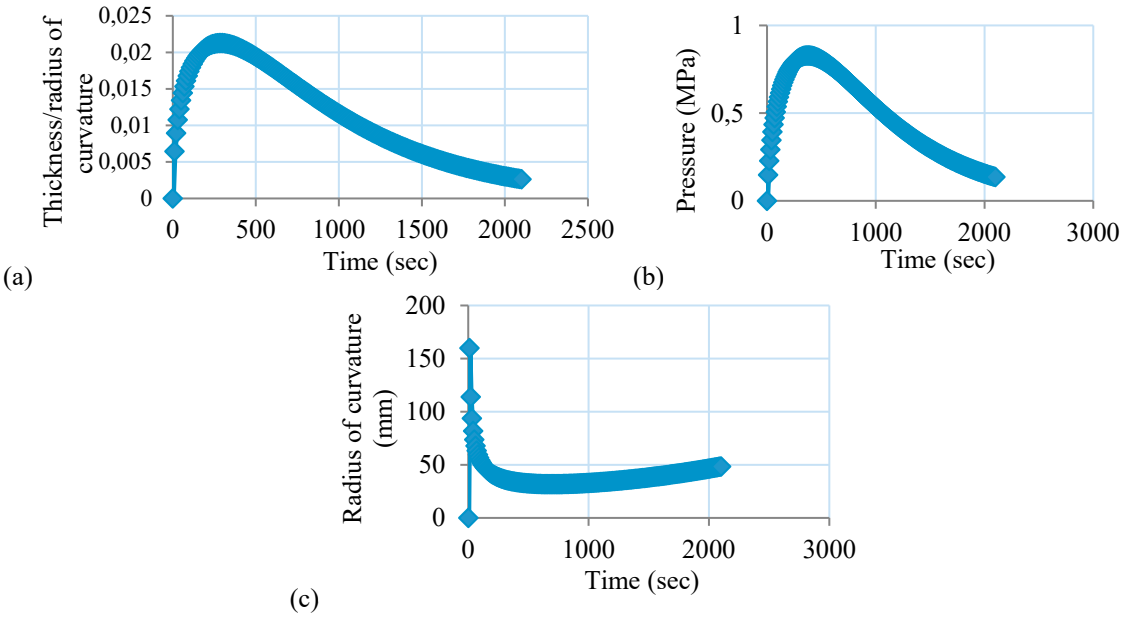

Figure3: (a) variation of the ratio of thickness to the radius of curvature with respect to time, (b) Variation of pressure with respect to time, (c) Variation of the radius of curvature with respect to time

It can be seen that the radius of curvature reaches 31.75 mm at forming time =690 sec =11.5 min, S/ρ = 0.016427 then S=0.52155 mm which is the minimum thickness. By comparing the simulation-based results of the material model without strain hardening with the analytical results for a strain rate of 1×10^{-3} 1/s, it can be found that the error for the minimum thickness is 1.64 %, which is a significant error relatively; the error should be less than 10%. According to the large error that we got, it is clear that the material model without strain hardening is not working, so a material model with strain hardening should be used. Another two material models were developed, one with a strain

rate of 1×10^{-3} 1/s and m=0.5 and another with a strain rate of 5×10^{-5} 1/s and m=0.66, where the values of m were according to the continuous and stepped averaged curves for m [1]. The power law equation of both strain and strain rate was found by the power curve fitting of a tensile data for an AZ31 alloy as shown in figure4, where the target strain rate was chosen to be 1×10^{-3} and 5×10^{-5} 1/s respectively.

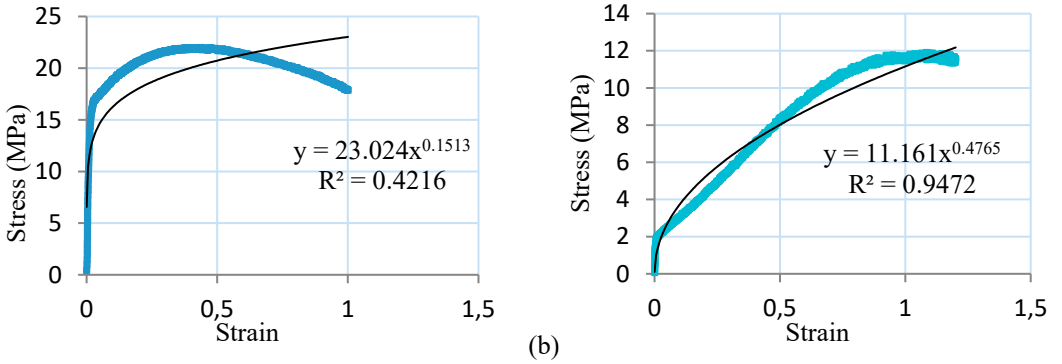

Figure4: (a) Power curve fitting for stress-strain curve with strain rate 0.001 1/s, (b) 0.00005 1/s

Material model variables were found using equations 9, 10, 11, 12, 13 and 14. For the material model with 0.001 1/s strain rate and m=0.5

- $n = \frac{1}{X+Y}$=1.535 (9)
- $m = \frac{-Y}{X+Y} = -0.2357$ (10)
- $A = \frac{1}{B^n(m+1)^m}$= 3.7935×10^{-5} (11)

For the material model with 0.00005 1/s strain rate and m=0.66

- $n = \frac{1}{X+Y}$=0.8799 (12)
- $m = \frac{-Y}{X+Y} = -0.4193$ (13)
- $A = \frac{1}{B^n(m+1)^m}$= 3.0297×10^{-4} (14)

Following the same procedure that was followed for the simulation of the bulge forming with a material model without strain hardening, the forming time was found to be 14.66 and 236.52 min, for the models with 1×10^{-3} and 5×10^{-5} 1/s strain rate respectively. While the experimental forming time was 14.68 and 231.17min for the models with 1×10^{-3} and 5×10^{-5} 1/s strain rate respectively. Figure5 shows thickness distributions with respect to the position along the die surface for the two material models respectively.

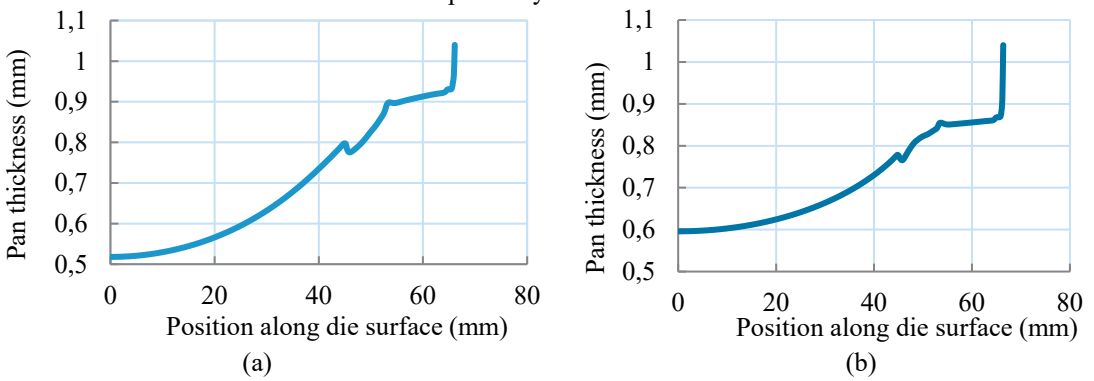

Figure5: (a) Thickness distribution with respect to position along die surface for a material model with 0.001 strain rate, (b) with 0.00005 strain rate

Finally, it was found that the model with 0.001 strain rates has an average thickness of 0.7036 mm, a minimum thickness of 0.5179 and a thinning factor of 0.736, while for the model with 0.00005 strain rates has an average thickness of 0.7139 mm, a minimum thickness of 0.5959 and a thinning factor of 0.835. In order to compare the results of the 0.00005 strain rate material model with analytical results, the same expression mentioned before for radius of curvature, the ratio of thickness to the radius of curvature and pressure were used, and it was found that the forming time is 231.17 min and the minimum thickness is 0.5197mm. Results of the above different cases are summarized in the following table to compare the different material models.

Table2: Summary for all the material models results

	Strain rate = 1*10^-3				Strain rate=5*10^-5		
	ABAQUS m=0.5	Analytical	Exp.	Without strain hardening	ABAQUS m=0.66	Analytical	Exp.
Forming time (min)	14.66	11.5	14.68	14.75	236.52	231.17	398.07
Average thickness (mm)	0.7036	_	_	0.7048	0.7139	_	_
Minimum thickness (mm)	0.5179	0.5216	_	0.5303	0.5959	0.5197	_
Thinning factor	0.7360	_	_	0.7524	0.835	_	_

The minimum thickness is the most important result in our research. Comparing it between simulation and analytical results will give the following errors:

- Without strain hardening: error= 1.66%
- 0.001 strain rate: error= 0.70%
- 0.00005 strain rate: error= 14.6%

So it is obvious that the best material model is the material model with a strain rate of 0.001 1/s and m=0.5.

3. Optimization of Hybrid Superplastic Forming of a Three-Stepped Die

HSPF technique has improved the utilization of SPF by forming is less time and less thinning by designing a technique that merges mechanical performing and gas pressurization in a single process. It was proved that the combining of mechanical pre-forming with conventional SPF is capable of forming SP alloys as AA5083 and non-SP alloys as AA5182 with less thinning and quicker forming time [16] [17]. Factors as die geometry, friction, and punch geometry have a significant influence on the success of the HSPF process. The diversity in the coefficient of friction between the die and sheet, punch and sheet and blank holder and sheet will straightaway influence the stress distribution of the formed material [19] [22].

3.1 Process Development

The hybrid SPF process will benefit from both mechanical and gas pressurization step to draw the sheet into the die cavity. The goal is to form a sheet of 100mm length and 0.82mm thickness into a three-stepped die (Figure6). This complex die geometry was chosen to show the advantages of using a hybrid SPF technique in the complicated cases that are almost impossible to form in one step without assembly using the conventional sheet forming methods. In

order to form more in-depth into the die at the first step, a two-stepped punch was used in the drawing phase with a speed of 0.6mm/s, and blank holder force was chosen to be 4 KN according to [28]. The pressure cycle was performed to hold the forming strain rate at 0.001/sec as targeted.

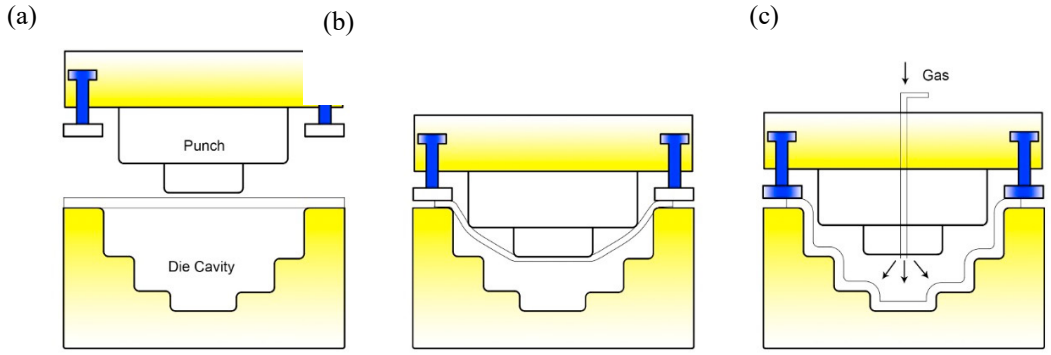

Figure6: Forming sequence of the hybrid SPF of an AZ31 alloy into a 3-stepped die using 2-stepped punch

In the hybrid SPF case, it is not necessary to have a punch geometry that matches the die geometry since it will not form the final shape of the die cavity. It is only used as a first step to form deeper through the die depth in a faster forming time, and then the gas pressure will continue to form the sheet into the die cavity. The die corner radius and the punch corner radius are the essential factors to perform an accurate deep drawing for the sheet into the die cavity, instead of shearing it. The edge radius affects the force distribution, which may cause the sheet to flow into the die cavity, so the die edge radius and punch edge radius was chosen to be 5mm and 12mm respectively. So the clearance used in this chapter was 0.9mm using a punch radius of 69.1mm and die radius of 70mm for the outer step even if it is not essential in this work since it contains the second step of superplastic forming, so it can have any punch radius that is found to be appropriate for the case. Amounts of deep drawing implemented on a metal sheet in one process are limited, and this is because of the geometry, metal flow, forces, and material properties. It has been shown by [26] that the limiting drawing ratio for AZ31 alloy under deep drawing at an initial blank temperature of 400 °C can reach 2.3, which means that the drawing ration, in this case, is acceptable. The tools including die, holder, and punch were modeled as rigid bodies. The AZ31 blank is modeled using axis-symmetric continuum four-node bilinear (CAX4I) which is an incompatible mode element; the incompatible mode elements have excellent bending properties. However, before deciding the element distribution of the sheet, a mesh convergence study was done as will be shown in the next section.

3.2 Mesh Convergence Study

It is substantial to use a mesh that is refined enough to guarantee that the outcomes from ABAQUS simulation are sufficient. Coarse meshes can produce inaccurate results through analyses. The numerical solution developed for the model will give an individual value with the increasing of the mesh density. When the mesh is refined, the computer resources that are essential to turn on the simulation will also increase. When further mesh refinement produces a minor change in the solution, the mesh is converged, which means that the model started producing a mathematical solution that is accurate enough [3]. The analysis was carried out using different mesh densities. In the vertical direction, two, three, four, six and eight elements within the sheet thickness were applied. Also, in the horizontal direction, different element sizes were applied to attain aspect ratio of 1.63.The first outputs are the von Mises stress at the top node of the sheet to the left side of the coordinate (0, 0.82), this is the moment where the sheet is entirely formed, and all the nodes are in contact with the die. The second output is the maximum in-plane principle stress at the node where it is supposed to be the weakest node in the formed part. After the first mesh trail, it was found that this node is (16.2, 0.82).Figure7 shows the different element distributions in the cases of 2,3,4,6 and 8 layers through

the thickness, keeping an element aspect ratio of 1.63, where according to [24] if the element has b length and thickness, then to avoid the element aspect ratio distortion it should be less than or equal to 10.

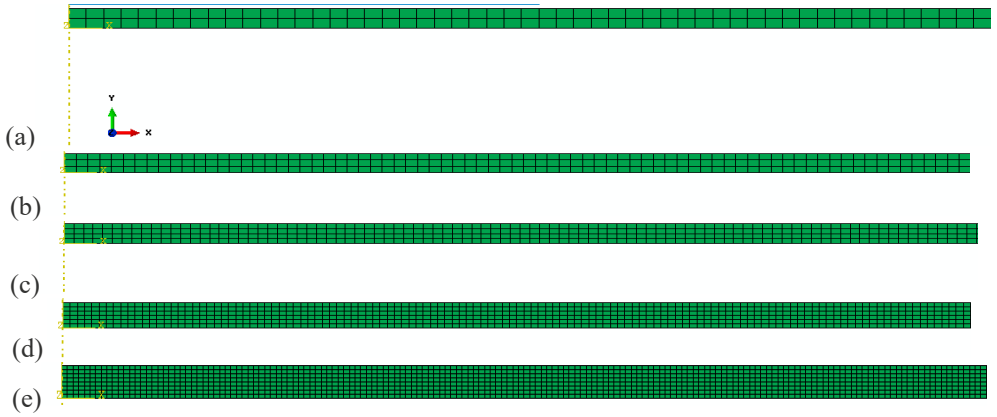

Figure7: Different meshes for (a) 2 layers, (b) 3 layers,(c) 4 layers,(d) 6 layers and (e) 8 layers through the thickness.

Finite element analysis was done on each case of the above meshes using the hybrid SPF technique to compose each sheet into a three-stepped die of the following geometry:

- Radius and depth of the 3rd (deeper) step= 25mm and 60mm respectively.
- Radius and depth of the 2nd step= 50 mm and 45mm respectively.
- Radius of the 1st step= 70 mm and 25mm respectively.
- Flange length= 30mm.
- Fillet radius for all corners= 5mm.

Table3 shows the x direct stresses; von Mises stresses at the top node of the sheet to the left side with the coordinate (0,0.82) at the moment where the sheet is entirely formed, and all the nodes are touching the die in each of the 5 cases. The percentage error was calculated between each case of meshing and the finer case, where the goal was to reach a relative error percentage that is equal or less than 0.5%.

Table3: Von Mises stresses/Mpa at (0.0.82) for different meshes

Element density through the sheet	Element density through sheet length	von Mises stress/Mpa at (0,0.82)
2	150	11.5933
3	225	11.8113
4	300	9.26106
6	450	9.99922
8	600	10.0267

The relative error percentages were calculated as follows:

- between 2 and 3 layers case: 1.88%
- between 3 and 4 layers case: 21.59%

- between 4 and 6 layers case: 7.97%
- between 6 and 8 layers case: 0.27%

The above results show the goal of percentage error less than 0.5% was reached after the 6 layers case mesh, which means that the convergence is reached using 6 layers through sheet thickness and 450 elements through sheet length. When the mesh is finer, then the computational time increases, so using this study we reached a mesh that satisfactorily balances accuracy and computing resources. After reaching the convergence by analyzing the von Mises stress at the point (0, 0.82), another analysis should be done on the weakest point of the part after forming. After the first trial, it was found that this point is (16.2, 0.82) which falls at the deeper corner of the die.

It is evident that convergence will not be reached with 2 or 3 layers cases, so the analysis for the von Mises stress at the weakest point starts from 4 layers within the sheet thickness and 300 elements through the sheet length. Table4 shows the von Mises stresses at the weakest node of the sheet with the coordinate (16.2, 0.82) at the moment where the sheet is entirely formed and all the nodes are in touching the die in each of the 3 cases. The goal was to reach a relative error percentage that is equal to or less than 0.5%.

Table4: Von Mises stresses/Mpa at (16.2, 0.82) for different meshes

Element density through the sheet	Element density through sheet length	von Mises stress/Mpa at (16.2,0.82)
4	300	19.2744
6	450	20.7726
8	600	20.6863

The relative error percentages were calculated as follows:

- between 4 and 6 layers case: 7.77%
- between 6 and 8 layers case: 0.41%

After reaching an error percentage less than 0.5%, it is concluded that the mesh defined as 6 elements within the sheet thickness and 450 elements through the sheet length is fine enough since the maximum stress is not changing appreciably.

3.3 Simulation of Hybrid SPF process

Deformed shapes that are predicted at various stages of the deep drawing and SPF steps for the AZ31 sheet into the 3-stepped die using 2-stepped punch are shown in figure8. The profiles show that the metal initially bends and stretches. Then drawn till it reaches 14 mm of the die depth in 23 seconds, then the pressure loading (SPF) starts till it reaches 60mm of the die depth in 1850 seconds, and all nodes became in contact with the die where it can be seen that filling the corner takes most of the time. Different aspect ratios were utilized to investigate the influence of changing the element aspect ratio on the simulation results. It was shown that after trying different aspect ratios, (350 elements through the sheet length and 6 elements through the sheet thickness (aspect ratio 2.09) and another with 600 elements through the sheet length and 6 elements through the sheet thickness (aspect ratio 1.22)), almost the same forming time was needed to form the sheet completely into the die.

The forming time for the 2.09 element aspect ratio was 23 sec for the first step and 1840 for the second step, and for the 1.22 element aspect ratio, it was 23 sec for the first step and 1880 sec for the second step. The conclusion that can be drawn from this simulation results is that the change in the element aspect ratio does not affect on the forming time of the process. The difference in meshing using 1.22, 1.63, 2.09 is not large, and the mesh is considered a fine mesh in the three cases and it still balancing between accuracy and computational effort, but using a coarse mesh may cause a large difference in the simulation results since it will not be accurate enough.

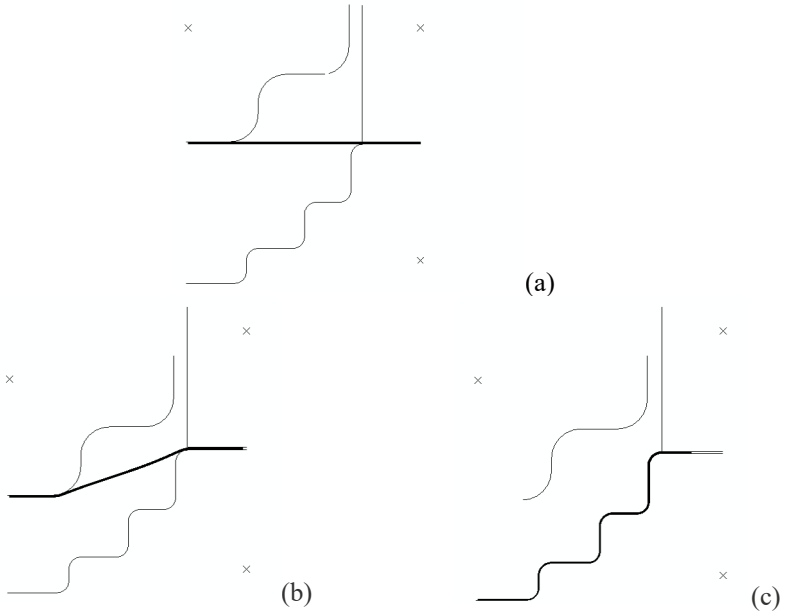

Figure8: Deformed shapes at (a) 0,(b) 23 and (c) 1850 sec for the 1.63 element aspect ratio

4. Parametric Study

A study that is based on finite element analysis was carried out to investigate the effect of the HSPF technique parameters on the forming time and distribution of formed sheet thickness. Parameters involve the punch geometry, blank holder force, drawing depth and punch speed. Table5 shows the values of the initial process parameters.

Table5: Values of the initial process parameters

The process parameters of the hybrid SPF process	
Punch speed	0.6 mm/s
Blank holder force	4 KN
Punch drawing depth	14 mm
Number of punch steps	2 steps
Punch fillet radius	12 mm
Punch outer step radius	69.1 mm
Punch inner step radius	30 mm
Punch outer step depth	30 mm
Punch inner step depth	30 mm

4.1 Influence of punch speed

Neglecting that there are many factors participate in influencing the quality of drawing, the highly effective element on the deep drawing operation of the sheet is the smoothness of sheet metal flow. Appropriate punching speed

grants time for materials to pass over the tool. If press speed is too fast, then corner cracking will regularly take place through the deep drawing technique. This simulation process was carried out with punch speed values such as 0.3 mm/sec, 0.6 mm/sec, 1 mm/sec and 3 mm/sec while other parameters have constant values. The different four simulation processes were done at a 4 KN holding force, 14 mm punch depth and a punch geometry of two steps and 12 mm filling radius where the punch radius was 70 and 30 mm for the outer and inner steps respectively and a 30mm depth for both steps of the punch. Table6 shows the simulation results for different punch speeds, where forming time, minimum thickness and maximum thinning were determined for each case. By analysing the results, it is shown that the speed of the punch has almost no effect on the forming time or maximum thinning in the present work as also shown in figure9 where it is clear that the thickness distribution profiles for different punch speeds are almost the same. The 0.6 mm/s has relatively the best results even if the difference in the forming time has not exceeded 60 seconds and 0.11% for maximum thinning.

Table6: Simulation results for different punch speeds

Punch speed (mm/s)	Forming time (sec)	Minimum thickness (mm)	Percentage of maximum thinning
0.3	1943	0.3420	58.29
0.6	1883	0.3429	58.18
1	1888	0.3425	58.23
3	1891	0.34260	58.21

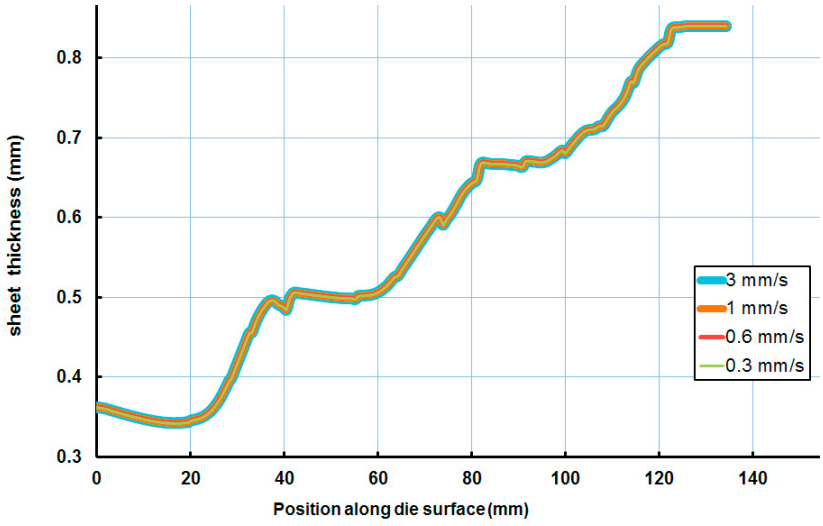

Figure9: thickness distribution for different punch speeds

4.2 Influence of blank holder force

In deep drawing, wrinkling and cracks have to be avoided by control of material flow. Blank holder force represents possibilities to influence material flow. The part may wrinkle during drawing if no force for the blank holder is used or if a blank holder force that is not sufficient is applied. Excessive blank holder force can produce a fracture. It is essential to investigate the effect of the blank holder force on the hybrid SPF technique and attain the value of the blank holder force that can be used without forming wrinkles for the sheet. FE simulation was performed

using five values of blank holder forces, 1, 2, 4, 10 and 30 KN. Boundary conditions were defined in a way similar to those defined before, with punch draw depth of 14 mm, punch speed of 0.6 mm/s and punch geometry of two steps and 12 mm filling radius where the punch radius was 70 and 30mm for the outer and inner steps respectively and a 30 mm depth for both steps of the punch.Table7 shows the simulation results for different blank holder forces, where forming time, minimum thickness and maximum thinning were determined for each case. By analysing the results, it is shown that the time of forming reduces with rising blank holder force, while the maximum thinning percentage increases with increasing of the blank holder force as also shown in figure10 where the minimum thickness is decreasing with the increase of the blank holder force. The 1 KN holding force has the best thinning percentage for the sheet, and the process has the longest forming time; it would be better to use a blank holder force of 1 KN.

Table7: Simulation results for different blank holder forces

Blank holder force (kN)	Forming time (sec)	Minimum thickness (mm)	Percentage of maximum thinning
1	2051	0.3708	54.78
2	2015	0.3597	56.13
4	1850	0.3429	58.18
10	1698	0.3064	62.63
30	1595	0.2768	66.24

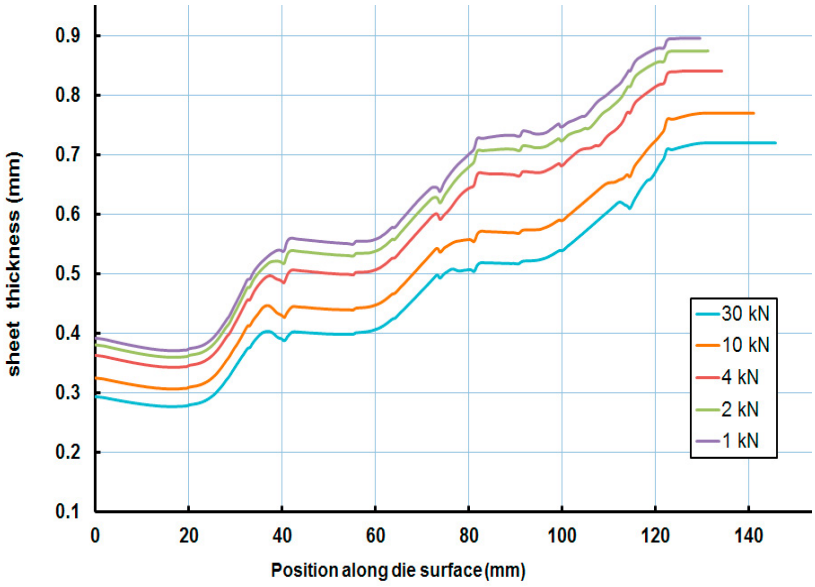

Figure10: Thickness distribution for different blank holder forces

4.3 Influence of punch draw depth and punch geometry

Finite element analysis was utilized for the modeling of the hybrid superplastic forming technique using three drawing depths, to examine the effect of pre-form drawing depth on the final thickness.10, 12 and 14 mm were the chosen punch depths since the punch depth is limited to avoid failure of the sheet. The influence of geometry for the punch on the final sheet thickness was also investigated. The investigation was carried out with three different sizes for the punch: 20, 30- and 45-mm. Boundary conditions were defined in a way similar to those presented before with

a force of 1kN for the blank holder. The study was done in a way where the possibilities of punch depth and punch geometry were considered as shown in Table8.

Table8: Parametric Details for all the possibilities of the study.

Study number	Draw depth (mm)	Punch Geometry (mm)	Punch speed (mm/sec)	Blankholder force (kN)
1	10	20	0.6	1
2	12	20	0.6	1
3	14	20	0.6	1
4	10	30	0.6	1
5	12	30	0.6	1
6	14	30	0.6	1
7	10	45	0.6	1
8	12	45	0.6	1
9	14	45	0.6	1

Figure11 presents the thickness distribution profile after the drawing step for the different draw depths with 20, 30- and 45-mm punch geometries respectively. By analyzing the figures and the results in Table9, it is shown that the maximum thinning decreases with increasing of the punch geometry.

Table9: Simulation results for different punch depth and geometry

Drawing depth(mm)	Punch geometry(mm)	Min. thickness(mm)	Percentage of max. thinning
10	20	0.806	1.7
12	20	0.801	2.3
14	20	0.796	2.93
10	30	0.807	1.58
12	30	0.803	2.07
14	30	0.800	2.4
10	45	0.808	1.4
12	45	0.804	1.95
14	45	0.801	2.3

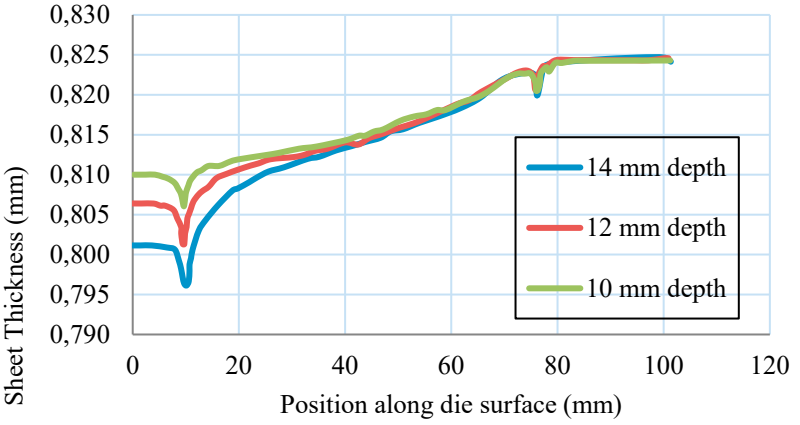

(a)

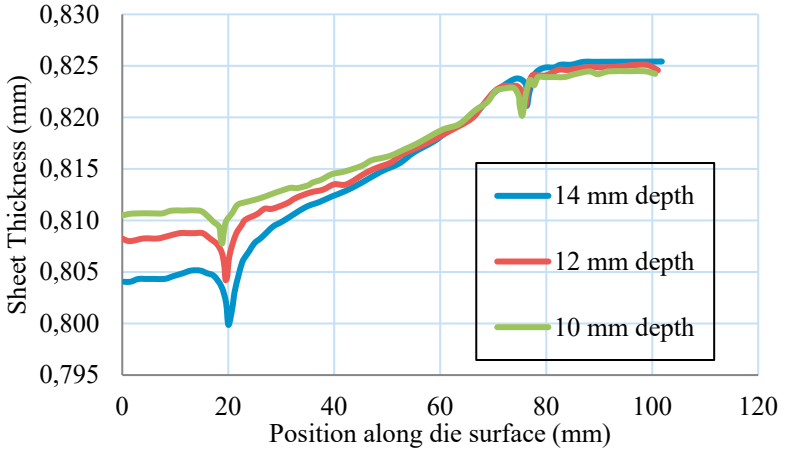

(b)

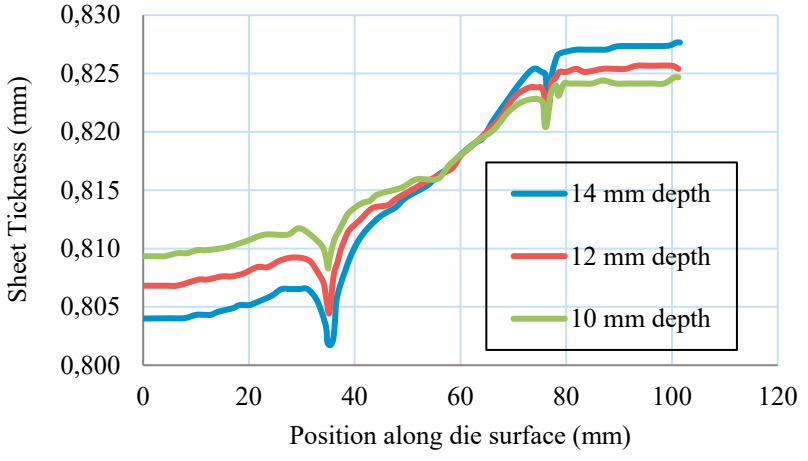

(c)

Figure11: (a) Thickness distribution at the end of the 1st step only for 20mm punch geometry, (b) 30mm punch geometry, (c) 45mm punch geometry

The thickness distribution profile was analyzed at the end of the hybrid SPF process for 10, 12 and 14mm punch depth using 45mm punch geometry. It was shown that the maximum thinning decreases with the increase of the punch geometry. Table10 shows the simulation results that show the effect of the punch depth on the overall forming time and thickness distribution. By analyzing the results, it is shown that the maximum thinning and the forming time decrease with the increase of the punch draw depth. The difference is not so clear in this case since we are limited in a relatively low punch draw depth to avoid failure of the sheet.

Table10: Simulation results for different draw depth

Drawing Depth (mm)	Forming time (sec)	Min. thickness(mm)	Percentage of max. thinning
10	2070	0.365	55.4
12	2038	0.368	55.1
14	2004	0.3708	54.7

As results, it can be concluded from the completely parametric study that the optimum parameters for the hybrid SPF process at a 400-Celsius forming temperature for both steps are as follows:

- 0.6 mm/s punch speed
- 1 kN Blankholder force
- 45 mm Punch geometry
- 14 mm punch draw depth

5. Results and Discussion

5.1 Comparison between conventional SPF and the optimum case of hybrid SPF process

Table11 lists the forming time for the hybrid forming process versus SPF. It took 2388 sec to form the cup using SPF technique only. Furthermore, it needs 2004 sec to shape the cup using the hybrid forming technique, which means it got a 384 sec (6.4 min) reduction in forming time. The first step (deep drawing) took only 23 sec to form 14 mm of the die depth, while the second step (SPF) took 1981 sec to form the last 46 mm of the cup. It is evident that utilizing the hybrid forming process can save a significant amount of time. The thickness distribution profile for both hybrid SPF and conventional SPF are shown in figure12.

Table11: Comparison in forming time between hybrid technique and SPF

Forming method	Forming time (sec)
SPF only	2388
Hybrid (preforming step)	23
Hybrid (SPF step)	1981
Hybrid total	2004

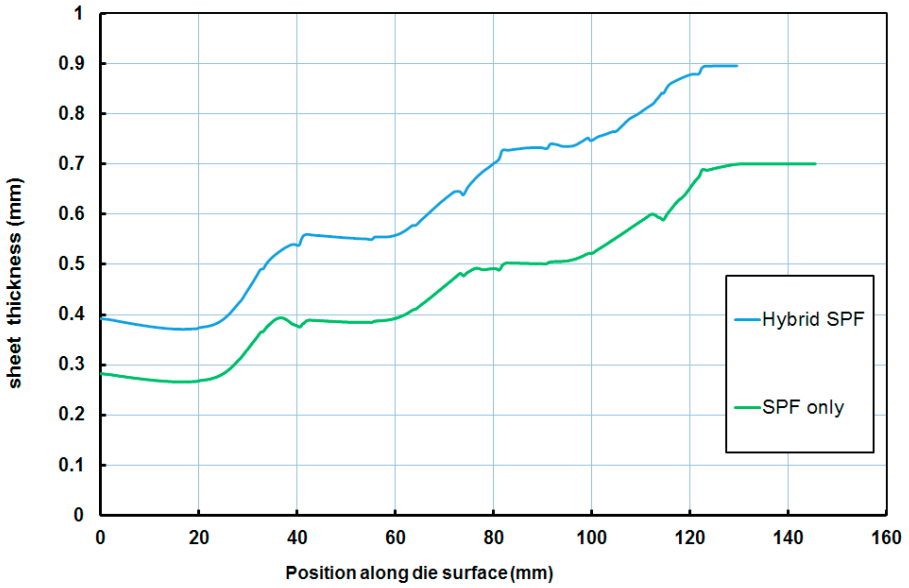

Figure12: Thickness distribution for both Hybrid SPF and SPF only process

It is seen from figure12 that more uniformity in thickness distribution is achieved for the 3-stepped die formed using the hybrid technique, where the minimum thickness was found to be 0.266 and 0.3708 mm for the SPF and hybrid technique respectively from an initial sheet thickness 0.82mm. It is seen that the final thickness is significantly improved where the maximum thinning was improved from 67.56% in SPF only to 54.78% using hybrid SPF technique.

5.2 Predicted gas pressure profile for optimum forming process parameters

Figure13 shows the predicted gas pressure profile with respect to time where it can be noticed that there is a sharp rise in the pressure of forming through the last steps, where the filling of the die corners occurs, since they require most of the forming time and the highest values of pressure through the whole hybrid SPF process.

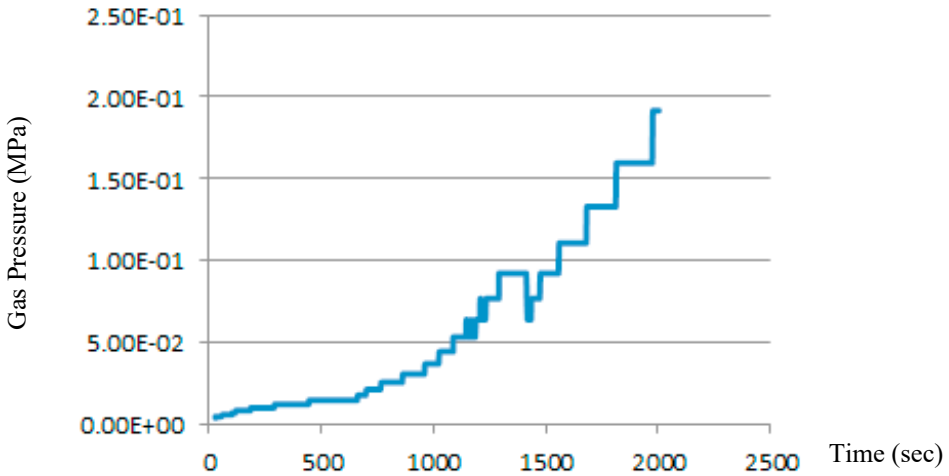

Figure13: Predicted gas pressure profile for the optimum process parameters in hybrid SPF

6. Conclusions

An SPF technique that uses a preforming mechanical punch was presented in this study. Finite element code including direct implicit integration was used through the analysis of the hybrid SPF trials with a simple cup to verify the benefits of the hybrid SPF process in reducing the forming time and improving the final sheet thickness distribution profile. Then it was used for the forming into a more complicated geometry that was chosen to be a three-stepped die. The effect of various parameters in the SPF technique was examined by discussing the differences in the simulation results regarding final thickness distribution where it delivered at the end an improved thickness profile and a considerable decrease in the time of forming by comparing it to the classic SPF technique. Specific conclusions include:

- Power creep law material model can be utilized for the precise modelling of the material draw-in and thinning of AZ31 alloy through conventional and Hybrid SPF technique.
- Mesh convergence study was made at 1.63 element aspect ratio where it was found that convergence is reached at a mesh with 450 elements through the sheet length and 6 elements through the sheet thickness.
- Hybrid SPF technique accomplished a time of forming of 1375 sec while conventional SPF needed 1559 sec during the forming of a simple cup and time of forming of 2004 sec while conventional SPF needed 2388 sec during the forming of a three-stepped die.
- Thinning of the material was cut in AZ31 alloy from 66.8% as a maximum percentage to 64.7% with the use of HDMP during the forming of a simple cup and a reduction from a maximum of 67.56% to 54.78% during the forming of the three-stepped die.

References

[1] Abu-Farha, F. (2007). On the superplastic forming of magnesium alloys: towards potential automotive applications. Unpublished Doctoral Dissertation, University of Kentucky, Lexington, Kentucky.

[2] Albakri, M. Jarrar, F. and Khraisheh, M. (2011), Effects of Interfacial Friction Distribution on the Superplastic Forming of AA5083. Journal of Engineering Materials and Technology, 133.

[3] ABAQUS 6.10, Example Problem Manual. Volume I: Static and Dynamic Analysis.

[4] ABAQUS 6.10, Getting Started with ABAQUS. Interactive Edition.

[5] Cahn, R. and Haasen, P. (1996), Physical Metallurgy, (4th edition). North-Holland.

[6] Carrino, L. Squillace, A. Paradiso, V. Ciliberto, S. and Montuori, M. (2013), Superplastic forming of friction stir processed magnesium alloys for aeronautical applications: a modeling approach. Materials Science Forum, 735, 180-191.

[7] Dutta, A. and Mukherjee, A. (1992), Superplastic forming: an analytical approach. Materials Science and Engineering, 157, 9-13.

[8] Ghosh, A. and Hamilton, C. (1980), Superplastic forming of a long rectangular box section-analysis and experiment. Process modeling; fundamentals and applications to metals. 303-331.

[9] Harrison, N. Luckey, S. Friedman, P. and Xia, Z. (2004), Influence of friction and die geometry on simulations of superplastic forming of Al-Mg alloys. Proceedings of Advances in superplasticity and superplastic forming, TMS, Charlotte, North Carolina, USA 14-18 March, 301-310.

[10] Jarrar, F. Abu-Farha, F. Hector, L. Jr., and Khraisheh, M. (2009), Simulation of high-temperature AA5083 bulge forming with a hardening/softening material model. Journal of Materials Engineering and Performance, 18(7), 863-870.

[11] Jovane, F. (1968). An approximate analysis of the superplastic forming of a thin circular diaphragm: Theory and experiments. International Journal of Mechanical Sciences, 10, 403-427.

[12] L. García-Barrachina, A.J. Gámez, and M. Marcos. (2017), Dimensionless analysis of superplastic bulge forming. Procedia Manufacturing, 13, 364–371.

[13] Liu, J. Ming-Jen, T. Jarfors, A. Lim, S. Fong, K. and Castagne, S. (2012), Greener manufacturing: Superplastic-like forming. Journal of Physics, 379.

[14] Liu, J. Tan, M. Aue-u-lan, Y. Jarfors, A. Fong, K. and Castagne, S. (2011), Superplastic-like forming of non-superplastic AA5083 combined with mechanical pre-forming. International Journal of Advanced Manufacturing Technology, 52, 123-129.

[15] Liu, J. Tan, M. Castagne, S. Aue-u- Lan, Y. Fong, K. and Jarfors, A. (2010), Investigation of Process Parameters in Superplastic Forming of Mechanical Pre-Formed Sheet by FEM. Key Engineering Materials, 447-448.

[16] Luo, Y. Luckey, S. Copple, W. and Friedman, P. (2008), Comparison of Advanced SPF Die Technologies in the Forming of a Production Panel. Journal of Material Engineering and Performance, 17, 142-152.

[17] Luo, Y. Luckey, S. Friedman, P. and Peng Y. (2008), Development of an Advanced Superplastic Forming Process Utilizing a Mechanical Pre-Forming Operation. International Journal of Machine Tools and Manufacture, 48, 1509-1518.

[18] Luckey, S. Friedman, P., and Xia, Z. (2004), Aspects of element formulation and strain rate control in the numerical modeling of superplastic forming. Proceedings of Advances in superplasticity and superplastic forming, TMS, Charlotte, North Carolina, USA 14-18 March, 371-380.

[19] Menezes, P. Kumar, K. and Kishore, K. (2009), Influence of friction during forming processes-a study using a numerical simulation technique. International Journal of Advanced Manufacturing Technology, 40, 1067-1076.

[20] Nazzal, M. Zaid, A. and Al-Qawabah, S. (2011), Finite Element Simulations of a Hybrid Forming Process: Deep Drawing and Superplastic Forming. Proceedings of 21st International Conference on Production Research, Stuttgart, Germany 31 July-4 August.

[21] Pan Wang, Shijie Zhu, Liguo Wang, Lihong Wu, Shaokang Guan (2015), A two-step superplastic forging forming of semi-continuously cast AZ70 magnesium alloy. Journal of Magnesium and Alloys, 3, 70-75.

[22] Park, D., and Yarlagadda, P. (2008), Effects of punch load for elliptical deep drawing product of automotive parts. International Journal of Advanced Manufacturing Technology, 35, 814-820.

[23] Park, K. Birt, M. and Mawella, K. (1996), Near net shape magnesium alloy components by superplastic forming and thixo forming. Advanced Performance Materials, 3, 365-375.

[24] Rao, S. (2005). The finite element method in engineering, (4th edition). Batterworth-Heinemann.

[25] Ritam Chatterjeea and Jyoti Mukhopadhyay. (2018), A Review of Superplastic forming. Materials Today: Proceedings, 5, 4452–4459.

[26] Sivanandini, M. Dhami, S. and Pabla, B. (2012), Formability of magnesium alloys. International Journal of Modern Engineering Research, 2(4), 2464-2471.

[27] S.Ramesh Babu, S. Deivanayagam and M. Aravind (2014), Determination of Material Parameters during Superplastic Forming of AA 5086 Alloy. Procedia Engineering, 97, 1379 – 1386.

[28] Tari, D. Worswick, M. Mckinley, J. and Bagheriasl, R. (2007), AZ31 magnesium deep drawing experiments and finite element simulation.
[29] Wert, J. (2004). Processing of superplastic Aluminum alloys. Riso National Laboratory.
[30] Z. Li, G. Dai1, J. Shi, F. Jarrar, F. Ozturk and J. Sheikh-Ahmad (2017). Using the particle swarm optimization method for the constitutive modeling of AZ31B. Mat.-wiss. u. Werkstofftech, 48, 993–997.